

1 Running head: Differential dissolution in coccolithophores

2 **Species-specific differential dissolution morphology of selected coccolithophore**
3 **species: an experimental study**

4 Gerald Langer^{1,2}, Ian Probert³, Jeremy R. Young⁴, Patrizia Ziveri^{1,5,6}

5 **Affiliations**

6 ¹ Institute of Environmental Science and Technology, Universitat Autònoma de
7 Barcelona (ICTA-UAB), Barcelona, 08193, Spain

8 ² Marine Biogeochemistry, Alfred Wegener Institute, 27570 Bremerhaven, Germany

9 ³ Sorbonne Université/CNRS, Roscoff Culture Collection, FR2424 Station Biologique
10 de Roscoff, 29682 Roscoff, France

11 ⁴ Earth Sciences, University College London, London WC1E 6BT, UK

12 ⁵ Catalan Institution for Research and Advanced Studies (ICREA), Barcelona, Spain

13 ⁶ BABVE Dept., Universitat Autònoma de Barcelona (ICTA-UAB), Barcelona, 08193,
14 Spain

15

16 Corresponding author: Gerald Langer (gerald.langer@cantab.net,
17 gerald.langer@awi.de)

18

19 **500-character summary**

20 Coccolithophores are important marine CaCO₃ producers and their biominerals, the
21 coccoliths, partly dissolve in the upper water column where dissolution is unexpected.
22 Studying coccolith dissolution in field samples is hampered by a paucity of
23 experimental studies describing dissolution morphologies. Here we fill this gap by
24 experimentally dissolving different coccolithophores and applying our results to field
25 samples.

26

27 **Highlights**

- 28 - Experimental studies on biogenic CaCO₃ dissolution provide novel insights into
29 field sample observations and biomineralization processes
- 30 - Experimental data aid the interpretation of aberrant coccolith morphology in
31 field samples
- 32 - In *C. braarudii* partial dissolution reveals a nanostructure in the distal shield
- 33 - The nanostructure in *C. braarudii* requires adjustments in biomineralization
34 models

35

36 **Abstract**

37 Coccolith dissolution in the water column is an important process in the marine carbon
38 cycle. Identifying dissolution in water column samples has been difficult due to a lack
39 of experimental reference datasets showing dissolution morphologies. We conducted a
40 laboratory CaCO₃ dissolution experiment to detect differential dissolution morphologies
41 of three selected coccolithophore (abundant marine calcareous phytoplankton) species,
42 *Coccolithus braarudii*, *Helicosphaera carteri*, and *Scyphosphaera apsteinii*. These
43 species were selected because they are ecologically and biogeochemically important
44 (significant contributors to CaCO₃ production) and have been less studied than
45 *Gephyrocapsa*. Murooliths of *S. apsteinii* dissolve faster than lopadoliths, which in turn
46 dissolve as fast as *H. carteri* but faster than *C. braarudii*. In *S. apsteinii* lopadoliths,
47 dissolution rate depends on the crystallographic orientation of the crystals. Comparison
48 with field samples shows that experimental data are helpful when interpreting field
49 samples. For example, we identify dissolution in water and sediment samples reported
50 in the literature. In *C. braarudii* dissolution reveals a nanostructure on the proximal side
51 of the distal shield, an observation that has implications for coccolith biomineralization
52 models, which do not currently account for the formation of such a structure. This
53 nanostructure features “units” of ca 50-100 nm and resembles the nanostructure well
54 known from extracellular calcifiers such as molluscs and foraminifera. Whether this
55 resemblance is underpinned by a similar formation mechanism remains unknown, but
56 we think this unlikely.

57

58 **1) Introduction**

59 Present anthropogenic CO₂ concentration changes, both atmospheric and marine,
60 cannot be fully understood without considering marine calcium carbonate, largely
61 produced by calcifying organisms (Broecker and Peng 1982, Morse and Mackenzie
62 1990). These calcifying organisms influence air-sea CO₂ exchange in several ways, e.g.
63 through particulate inorganic- and organic carbon production in the surface ocean but
64 also through export of calcium carbonate to the deep ocean (Morse and Mackenzie
65 1990). The most productive marine calcium carbonate (CaCO₃) producers are pelagic
66 organisms, with coccolithophores contributing ca. 90% of global pelagic CaCO₃
67 production (Ziveri et al., 2023) and ca. 50% of CaCO₃ sedimentation (Milliman 1993,
68 Broecker and Clark 2009). Dissolution of CaCO₃ in the photic zone is an important
69 process in the marine CaCO₃ cycle (Ziveri et al. 2023; Subhas et al. 2022; Sulpis et al.
70 2021). The importance of dissolution for the marine C-cycle has two main aspects.
71 Firstly, dissolution of CaCO₃ releases two moles of alkalinity per one mole of dissolved
72 inorganic carbon, thereby shifting the seawater C-system towards higher pH values
73 (Zeebe and Wolf-Gladrow, 2001). Secondly, the loss of ballast minerals reduces carbon
74 export efficiency thereby influencing the C-cycle long-term (Klaas and Archer 2002). In
75 addition to occurring in the open ocean photic zone, dissolution of carbonates in
76 general, and coccoliths in particular, may also occur in sediments and coastal CO₂ vent
77 sites (Honjo 1975, Ziveri et al 2014).

78 Assessing coccolith dissolution in these diverse settings can be challenging, but partial
79 dissolution morphologies as identified in electron micrographs have proved a useful tool
80 (e.g. Langer et al 2007, Ziveri et al 2014). Knowledge of such differential dissolution
81 morphologies will aid interpretation of field samples, e.g. the degree of dissolution in
82 one species will inform inferences about the degree of dissolution in other species.
83 More fundamentally, knowledge about dissolution morphologies will enable us to
84 accurately distinguish malformation / under-calcification from dissolution, which is not
85 necessarily an easy task (Young 1994). Finally, dissolution might reveal informative
86 structural features (Langer et al 2007). The main goal of our study is to provide a
87 dissolution-morphology reference dataset which can be used to identify dissolution in
88 water column samples. The applicability of our data to sediment samples might be more
89 limited as discussed below. The interpretation of field samples is difficult, however,
90 because the degree, and even the mere fact, of dissolution often need to be inferred from
91 the micrographs alone, without precise knowledge of the physico-chemical conditions

92 leading to the observed morphology. For example, in surface sediments *Calcidiscus*
93 *leptoporus* coccoliths (placoliths characterized by two shield-like plates connected by a
94 central tube) lacking proximal shields have been taken as a sign of heavy dissolution
95 (Roth and Berger 1975), which has been proposed as a proxy for dissolution in the
96 sedimentary record (Matsuoka 1999). Only an experimental study could show that
97 separation of the shields is the first observable dissolution feature occurring at less than
98 8% mass loss (Langer et al 2007) revealing the “weak spot” at the proximal end of the
99 tube (the position of the proto-coccolith ring, Young et al 2004).

100 Despite the importance of experimental studies showing graded dissolution of
101 coccoliths, only a few such studies have been conducted (McIntyre & McIntyre 1971,
102 Burns 1977, Kleijne 1990, Henriksen et al 2004, Langer et al 2006b, Holcová and
103 Scheiner 2023), with a focus on *Gephyrocapsa* spp, in particular *G. huxleyi*, a widely
104 used model species (Wheeler et al 2023). The degree of dissolution in *G. huxleyi* water
105 column samples is difficult to assess as there are variations of progressive dissolution
106 patterns with e.g. warm- and cold-water phenotypes (Burns 1977). The latter author
107 pointed out that a tropical *G. huxleyi* loses the central grille in the first stages of
108 dissolution, while a cold-water phenotype does not. Calcite removal from the long
109 margin of the radial elements is a sign of early dissolution in the cold-water phenotype
110 but not in a heavily calcified phenotype. These and similar observations made by Burns
111 (1977) show that assessing the degree of dissolution in *G. huxleyi* is not an easy task
112 and morphotype-specific assessments are required. While *G. huxleyi* is numerically the
113 most abundant coccolithophore in present oceans, its contribution to coccolithophore
114 CaCO₃ production is rivalled by some genera with larger coccoliths, such as *Calcidiscus*
115 and *Coccolithus* (Wheeler et al 2023). The relatively recent appearance of *G. huxleyi* in
116 the fossil record implies that this species is not applicable to deep time sediment core
117 studies (Henderiks et al 2022). It is therefore worthwhile also studying genera with
118 larger coccoliths and mass, biogeochemically important (Ziveri et al., 2004), and with a
119 more extensive evolutionary history, e.g. *Coccolithus*, *Helicosphaera*, and
120 *Scyphosphaera* (Henderiks et al 2022). The latter genera are not as abundant as *G.*
121 *huxleyi* but play an important role in coccolithophore CaCO₃ production and export in
122 modern oceans (Baumann et al., 2004; Daniels et al., 2014, 2016; Gafar et al., 2019;
123 Ziveri et al., 2007).

124 Based largely on field sediment studies, it is accepted that some coccolith forms
125 dissolve faster than others. While *G. huxleyi* and *Umbilicosphaera sibogae* are among
126 the fast-dissolving placolith bearing species, *G. oceanica*, *C. leptoporus*, and *C.*
127 *pelagicus* are comparatively slow-dissolving (McIntyre & McIntyre 1971, Berger 1973,
128 Roth and Coulbourn 1982). These studies have not assessed how dissolution
129 morphologies of different species relate to each other. In other words, which dissolution
130 morphology of species x corresponds to a given dissolution morphology of species y?

131 Coccoliths contain crystals of different orientations, sizes, and shapes. A typical feature,
132 for example, is the presence of crystals with radial c-axis orientations (R-units) and
133 others with vertical c-axis orientations (V-units, Young et al 1992). It might therefore be
134 hypothesized that different crystals display different structural features, not only on the
135 micrometre but also on the nanometre scale. Some of these features might only be
136 discernible in partially dissolved specimens.

137 In this study we selected laboratory cultures of *Coccolithus braarudii*, *Helicosphaera*
138 *carteri*, and *Scyphosphaera apsteinii*, and performed a dissolution experiment to follow
139 their differential dissolution morphologies by means of sequential sampling for SEM
140 analysis. Here we analyse two important aspects of dissolution. Firstly, the selective
141 dissolution of different species relative to each other. Secondly, the evolution of
142 morphology of a given species with progressive dissolution. We hypothesize that
143 dissolution morphologies will be different from malformations (Bianco et al 2025,
144 Langer et al. 2006, Langer et al 2021, Gerecht et al 2015, Meyer et al 2020) and
145 therefore a dissolution reference dataset will enable us to unambiguously identify
146 dissolution in field samples. The experimental setup chosen here is ideally suited to
147 analyse sequential dissolution morphology with nanometric resolution. This enables the
148 identification of different dissolution stages in field samples, providing additional
149 information over and above the mere distinction of dissolution features and
150 malformations.

151 Experimental dissolution studies provide a good source of information on the evolution
152 of morphology with dissolution, without confounding factors from field studies such as
153 variance in the primary biomineralization morphology.

154

155 2) Material and Methods

156 2.1) *Culture conditions*

157 Clonal cultures of *Coccolithus braarudii* (strain RCC1198), *Scyphosphaera*
158 *apsteinii* (strain RCC3598), and *Helicosphaera carteri* (strain RCC1323) were grown in
159 aged (3 months), sterile-filtered (Stericup-GP Sterile Vacuum Filtration System, 0.22 μm
160 pore size, polyethersulfone membrane, Merck) natural surface seawater sampled in the
161 English Channel off Roscoff, France, enriched with 288 μM nitrate, 18 μM phosphate,
162 and silicate, trace metals, and vitamins as in Keller et al (1987) with the following
163 modifications: Cu and TRIS are omitted, $\text{NiCl}_2 \cdot 6\text{H}_2\text{O}$ 0.00314 μM is added, KH_2PO_4 is
164 used as P source. All strains were obtained from the Roscoff Culture Collection
165 (<http://www.roscoff-culture-collection.org>).

166 Cultures were grown under a 16:8 h light:dark cycle at a light intensity of
167 50 $\mu\text{mol photons m}^{-2} \text{ s}^{-1}$ in temperature-controlled culture incubators. *Coccolithus*
168 *braarudii* RCC1198 was grown at 15°C, while *Scyphosphaera apsteinii* RCC3598 and
169 *Helicosphaera carteri* RCC1323 were grown at 20°C. Cells were grown in dilute batch
170 cultures, ensuring a quasi-constant seawater carbonate system over the course of
171 exponential growth (Hoffmann et al. 2015). Cell densities were determined by flow
172 cytometry immediately after sampling. Cultures used in the dissolution experiment were
173 initially checked by light and scanning electron microscopy to ensure that coccosphere
174 morphology was normal (as observed in light microscopy) and the percentage of
175 coccolith malformations was below 15% (as determined by SEM analysis, Langer and
176 Bode 2011). The latter is a very low percentage of malformations in cultures (in which
177 values up to 90% have been reported, Langer et al 2006, Langer et al 2013), enabling
178 this study to focus on normal coccoliths and their dissolution morphologies, as opposed
179 to the dissolution features of malformed coccoliths (Langer and Bode 2011, Langer et al
180 2013, Langer et al 2023). We chose not to analyse the dissolution morphology of
181 malformed coccoliths because results are intended to be applicable to field samples, in
182 which the percentage of malformed coccoliths is typically only ca. 2% (Langer et al
183 2006, Langer et al 2013). Analysis of the dissolution morphologies of malformed
184 coccoliths would require a different experimental setup, with cultures displaying high
185 proportions of malformed coccoliths. Such an approach would be interesting in itself,
186 but does not fall within the scope of the present study (Langer et al 2006).

187 2.2) *Dissolution experiment*

188 To study differential dissolution morphologies accurately, the selected species
189 were combined in a single 2.7L bottle (Holcová and Scheiner 2023), in which case only
190 one calcite saturation state (ω) value can be selected. In pre-experiments we found
191 that *Gephyrocapsa huxleyi* coccoliths dissolved more than 10x faster than coccoliths of
192 *Coccolithus braarudii*, *Helicosphaera carteri*, and *Scyphosphaera apsteinii*, meaning it
193 was not possible to include *G. huxleyi* in our experiment. The three other species, *C.*
194 *braarudii*, *H. carteri*, and *S. apsteinii*, displayed broadly similar dissolution kinetics and
195 were therefore suited for our purpose.

196 To start the dissolution experiment, living cells were transferred into a 2.7L bottle
197 containing culture medium that was acidified using calculated amounts of HCl (3.29M)
198 immediately prior to cell transfer. We used acidification to manipulate ω calcite
199 because it is more representative of dissolution scenarios in the field than changes in Ca
200 concentration. ω calcite is the saturation state of seawater with respect to calcite,
201 with $\omega < 1$ indicating dissolution and $\omega > 1$ potential crystal growth. This
202 decision is important because the manipulation of ω calcite via acidification is
203 more effective than via Ca concentration decrease (Hassenkam et al 2011). We chose to
204 work with living cells, as opposed to isolated coccoliths for the following reasons.
205 Firstly, we wanted our results to be useful for comparison with various dissolution
206 scenarios such as whole cells in copepod and micro-grazer guts, whole cells in marine
207 snow aggregates, whole cells in ocean acidification-affected corrosive waters. Secondly,
208 we wanted to analyse effects of dissolution on coccospheres, as opposed to only on
209 individual coccoliths. Thirdly, removing coccoliths from cells is not always an easy task
210 and often requires chemical or heat treatment which might alter structural integrity and
211 organic content (Manuela Bordiga, personal communication, 2025). Since this is a pilot
212 study, we wanted to keep the experimental setup as straightforward as possible. Follow
213 up studies should deal with modified setups to explore additional factors influencing
214 dissolution patterns. The culture medium prepared using natural surface seawater
215 sampled off Roscoff, France has a typical dissolved inorganic carbon, DIC, of ca 2000
216 $\mu\text{mol kg}^{-1}$ (Johnson et al 2022). We used this value for DIC and measured pH (NBS) =
217 6.44 to calculate ω calcite = 0.033 using the program CO2SYS (Pierrot et al 2011).
218 The calculated value for ω calcite (0.033) was therefore approximate. However,
219 DIC variability of natural surface seawater sampled off Roscoff, France is low, therefore
220 introducing only a negligible inaccuracy in calculated ω calcite in the context of

221 the present study, i.e. an error of ± 0.005 is expected (Johnson et al 2022). The present
222 study was not designed to analyse dissolution kinetics precisely (such as in Subhas et al
223 2018), meaning an approximate determination of the carbonate system is sufficient. We
224 used a Cyberscan 500 pH meter (Eutech Instruments, UK) equipped with a Mettler
225 Toledo InLab 413/ID67 electrode to determine pH on the NBS scale.

226 Experimental dissolution over a very short space of time (on the order of seconds as in
227 Yang et al 2021) only allows for comparatively low-resolution light micrographs that
228 would have been insufficient for our purpose. The advantage of a short experiment
229 duration, however, is that DIC uptake and gas exchange with the atmosphere, and
230 therefore carbonate system variability, is negligible. Our dissolution experiment,
231 conducted over a duration of 11 hours, was carried out in the dark at 4°C to ensure that
232 cellular metabolism (including photosynthesis and coccolith production) was severely
233 restricted over the course of the experiment. Cell densities were 711 cells/mL for *C.*
234 *braarudii*, 665 cells/mL for *H. carteri*, and 586 cells/mL for *S. apsteinii*. The resultant
235 low overall cell density of 1963 cells/mL contributed to ensuring a quasi-constant
236 carbonate system over the course of the experiment (Langer et al 2006, Langer and
237 Bode 2011, Hoffmann et al 2015). Physico-chemical conditions over the course of the
238 experiment were additionally homogenized by regular mixing, i.e. keeping the cells in
239 suspension. No aggregation of cells occurred and no sedimentation of cells or coccoliths
240 took place. The pH did rise by ca 0.1 over the course of the experiment, but this
241 corresponds to an increase in omega calcite of only ca. 0.005, i.e. the same magnitude as
242 the minor uncertainty introduced by our choice of DIC value (see above).

243 After the dissolution experiment was completed, cells were transferred into normal
244 culture conditions as specified above. All three species, *C. braarudii*, *H. carteri*, and *S.*
245 *apsteinii*, resumed cell division and coccolith production as confirmed by optical
246 inspection using light microscopy. We did not quantify coccolith morphology in re-
247 calcifying cells, but noted that initially coccoliths seemed to display more
248 malformations than prior to the dissolution experiment. This assessment is based on an
249 informal analysis by means of light microscopy; no images were taken.

250 Multiple (15) sequential samples for detailed morphological analysis were taken over
251 the 11 hour duration of the experiment. Samples for SEM analysis were filtered onto
252 polycarbonate filters (0.8 μm pore-size), dried in a drying cabinet at 50°C for 24 h, then
253 sputter-coated with gold-palladium using a Cressington 108 sputter coater (Cressington

254 Scientific Instruments, Watford, UK). Imaging was performed with a Phenom Pro
255 desktop SEM at the Station Biologique de Roscoff, France, and an EI SEM Zeiss Merlin
256 at UAB, Barcelona, Spain. All the morphological features described in this study are
257 discernible using the Phenom Pro desktop SEM. We used the Zeiss Merlin FE-SEM
258 only to produce images showing the nanostructure on the proximal side of the distal
259 shield of *C. braarudii* because the latter microscope has a higher resolution. This
260 nanostructure, however, was discovered using the Phenom Pro desktop SEM. An
261 average of ~350 coccoliths was analysed per sample (Langer and Benner 2009). To
262 describe dissolution morphologies, we selected conspicuous features that could be
263 easily followed over the course of the experiment to ensure robust results and to
264 facilitate application to field samples. In *C. braarudii* and *H. carteri* we analysed
265 dissolution features of coccospheres in addition to dissolution features of coccoliths. In
266 *S. apsteinii* only dissolution features of coccoliths were analysed because coccospheres
267 in this species lack the mechanical stability needed to consistently withstand the
268 mechanical forces experienced in SEM preparation (Langer et al 2023). The following
269 morphological features were used to describe dissolution. In *C. braarudii*: 1) etching of
270 the inner tube, 2) etching of the distal shield, 3) central area bar missing, 4) coccoliths
271 broken, 5) gaps in coccospheres, 6) coccospheres collapsed, 7) nanostructure visible (on
272 proximal side of distal shield). In *H. carteri*: 1) etching, 2) coccoliths broken, 3)
273 coccospheres collapsed. In *S. apsteinii* lopadoliths: 1) etching of base, 2) etching of
274 barrel, 3) rim serrated, 4) lopadoliths broken, 5) isolated lopadolith V units. In *S.*
275 *apsteinii* muraliths: 1) centre missing, 2) etching, 3) muraliths broken. Scanning
276 electron micrographs of all of these features are shown in Figs 1-5. The most important
277 dissolution features for practical purposes are summarised in Table 1.

278

279 **3) Results and Discussion**

280 *3.1) Differential dissolution: general observations*

281 We subjected living cells of three common coccolithophore species, namely
282 *Coccolithus braarudii*, *Helicosphaera carteri*, and *Scyphosphaera apsteinii*, to seawater
283 undersaturated with respect to calcite, i.e. omega calcite ca. 0.033 (see Methods). The
284 duration of the experiment was 11 hours, at the end of which only a few isolated distal
285 shield elements of *C. braarudii* remained (Fig 6). Our observation that *C. braarudii* is

286 more dissolution resistant than *H. carteri* tallies well with conclusions drawn from
287 studying Atlantic Ocean floor sediments (Berger 1973). Information on *S. apsteinii* in
288 differential dissolution studies is rare, with this species either only mentioned but not
289 discussed or not mentioned at all (McIntyre & McIntyre 1971, Berger 1973, Roth and
290 Coulbourn 1982). From our data we conclude that *S. apsteinii* lopadoliths display
291 dissolution kinetics similar to *H. carteri*, while *S. apsteinii* muroliths dissolve faster. In
292 *S. apsteinii*, R-units, which are smaller and radially oriented, dissolve conspicuously
293 faster than the larger, vertically oriented V-units (Figs 6, 7, see also Drescher et al
294 2012). Since lopadoliths contain calcite only, as opposed to e.g. aragonite (Walker et al
295 2024), the latter observation illustrates that differential dissolution kinetics of biogenic
296 calcium carbonate cannot be inferred from the polymorph only (Langer and Ziveri
297 2025). Both etching and broken coccoliths appear simultaneously in *S. apsteinii*
298 lopadoliths and *H. carteri* (Figs 6, 7). In *C. braarudii* etching of the inner tube occurs
299 simultaneously with etching in *H. carteri* and *S. apsteinii*, but etching of the *C.*
300 *braarudii* distal shield appears later, possibly because the latter features the largest
301 crystals (Figs 6, 7). Relatively slow dissolution of the distal shield compared to the
302 tube/central area was also observed in *C. leptoporus* and might be a general feature of
303 Coccolithales placoliths (Langer et al 2007).

304 3.2) Comparison with field samples

305 Identification of dissolution in field samples:

306 As noted in the introduction coccolith dissolution in the water column is being
307 highlighted as a key process, greatly affecting the export production of coccolith CaCO_3
308 to the bottom sediment. Our experimental results on the sequence of dissolution stages
309 might usefully be applied to study of field samples in order to analyse and track water
310 column dissolution. As a proof of concept we show here (Fig 8) images of *Coccolithus*
311 *braarudii* and *Helicosphaera carteri* coccoliths from sediment trap samples and of
312 coccoliths from water column samples, in both cases showing dissolution features
313 directly comparable to those we observed experimentally. It is also noteworthy that the
314 nanostructure seen in the experimental samples is visible in the field samples (Fig 8)
315 showing that it is not an experimental artefact. Comparable dissolution features have
316 also been illustrated in the literature, for example by Cubillos et al (2012) and Kleijne
317 (1990), although in some cases they have been ascribed to malformation.

318 It is striking that in the three species studied here dissolution morphologies are clearly
319 different from malformations. The latter do not resemble etching as described here (Figs
320 1-5). This is remarkable considering that it has typically been difficult to distinguish
321 dissolution from malformation, and even fracture, in *G. huxleyi* (McIntyre & McIntyre
322 1971, Burns 1977, Kleijne 1990, Holcová and Scheiner 2023, Young 1994, Langer et al
323 2006b, Langer and Benner 2009, Langer et al 2011). These difficulties in identifying
324 dissolution morphology in *G. huxleyi* are particularly conspicuous in morpho-type B/C,
325 but are clearly noticeable in type A as well (own observations, unpublished). It might be
326 speculated that dissolution is easier to identify in type R because the latter features
327 fused distal shield elements which makes the overall morphology more similar to the
328 one of the species studied here. This conjecture is supported by *G. huxleyi* morphotype-
329 specific dissolution morphologies described in water column samples (Burns 1977). It
330 will be worthwhile studying different *G. huxleyi* morphotypes in greater detail. Species-
331 specific dissolution features such as the serrated rim in *S. apsteinii* lopadoliths are also
332 dissimilar to malformations such as type R (Langer et al 2021, Langer et al 2023). The
333 nanostructure on the proximal side of the distal shield of *C. braarudii* is hardly visible
334 in normal as well as malformed coccoliths, whereas it is clearly visible in partially
335 dissolved coccoliths. In *C. braarudii* a concentric hole sometimes appears in malformed
336 coccoliths (Langer et al 2021). This hole is clearly different from etch pits. A typical
337 feature of more severe malformations in placolith bearing species is the distorted
338 architecture of the shields (Bianco et al 2025, Langer et al 2006, Langer and Benner
339 2009, Langer et al 2011, Langer and Bode 2011, Langer et al 2012, Langer et al 2013,
340 Langer et al 2021, Langer et al 2023, Kottmeier et al 2022, Gerech et al 2015, Milner et
341 al 2016, Johnson et al 2022) which does not occur as a result of dissolution.

342 Do the conditions under which dissolution occurs influence dissolution
343 morphologies?

344 As a caveat we will say that dissolution morphologies might well depend on the
345 conditions under which dissolution occurs. For example, the presence or absence of an
346 organic coating around coccoliths results in slightly different dissolution morphologies
347 as seen in high resolution AFM imaging (Henriksen et al 2004). Since we did not
348 remove the organic coating, our results should be best applicable to water samples (with
349 organic coating) as opposed to sediment samples (in which the organic coating might be
350 degraded). That said, the organic coating of coccoliths can still slow down dissolution

351 after 70Ma in the sediment (Sand et al 2014). Whether dissolution morphologies of
352 these ancient coccoliths would be similar to those of cultured specimens remains to be
353 tested. A good candidate would be *C. pelagicus* because it first appeared in the fossil
354 record more than 60 Ma (Henderiks et al 2022). Another aspect to consider is the way
355 undersaturation is achieved. Dissolution kinetics in low-Ca solutions are different from
356 those in low-pH solutions (Hassenkam et al 2011). It is an open question whether
357 dissolution morphologies would differ too. In addition, pressure-driven undersaturation
358 might be relevant for deep-sea sediment samples. All of these issues are amenable to
359 experimental testing and should be the focus of future studies.

360 3.3) Structural integrity of the coccosphere

361 An interesting difference between *C. leptoporus* (Langer et al 2007) on the one
362 hand and *C. braarudii* / *H. carteri* (this study) on the other hand is the structural
363 integrity of coccospheres under dissolution. The earliest feature of dissolution in *C.*
364 *leptoporus* dissolved at an omega calcite of 0.5, is the separation of the shields resulting
365 in coccosphere collapse (Langer et al 2007). By contrast, in *C. braarudii* and *H. carteri*
366 the earliest dissolution feature is etching leaving the coccospheres intact. Only when
367 coccoliths break due to more pronounced etching do coccospheres collapse in these
368 species (Fig 7). This means that living *C. leptoporus* cells are more vulnerable to
369 dissolution than *C. braarudii* / *H. carteri* because all three species need a coccosphere
370 to live (Walker et al 2018a, Bianco et al., 2025). While a coccosphere comprised of
371 coccoliths produced by the very cell itself is essential for survival in monospecific
372 cultures of these species, mixed-species coccospheres in natural assemblages indicate
373 that coccosphere integrity can be re-established or modified through incorporation of
374 foreign coccoliths (Johns et al 2023). This might mean that a coccosphere compromised
375 through dissolution or malformation might be repaired by incorporating foreign
376 coccoliths. The protective efficacy of such hybrid coccospheres remains to be tested
377 experimentally. However, the vulnerability sequence described above differs from what
378 would be expected based on species specific coccolith solubility as inferred from
379 sediment samples, which do not suggest that *C. leptoporus* is more vulnerable than *H.*
380 *carteri* (Berger 1973). Note that we cannot be entirely sure that *C. leptoporus* coccoliths
381 would break faster than *H. carteri* coccoliths when subjected to the same omega calcite
382 because the *C. leptoporus* experiment was conducted at an omega calcite of 0.5 (Langer
383 et al 2007) as opposed to the ca 0.033 used here. Nevertheless, considering the very

384 early appearance of separated shields in *C. leptoporus* (Langer et al 2007) and the
385 comparatively late appearance of broken coccoliths in *H. carteri*, it is highly likely that
386 coccosphere collapse in *C. leptoporus* would occur earlier than in *H. carteri* (at a given
387 omega calcite). Although bulk surface waters in most parts of the global ocean are
388 currently supersaturated with respect to calcite, ongoing ocean acidification drives the
389 calcite saturation state towards undersaturation which will be reached in some areas,
390 e.g. the Southern Ocean, around the year 2100, posing a threat to calcifying organisms
391 including coccolithophores (Langer and Ziveri 2025). Please note that most surface
392 waters will remain supersaturated with respect to calcite, so that our results are most
393 directly relevant to locally undersaturated conditions (e.g. upwelling regions, eddies,
394 sea-ice melt, or pore waters). Regardless of the actual threat posed by corrosive waters
395 to living coccolithophores, the argument we are making here centres on relative
396 vulnerability of different species in case of calcite undersaturation.

397 3.4) *A nanostructure in C. braarudii biomineral*

398 A nanostructure on the proximal side of the distal shield in *C. braarudii* became
399 visible 3 hours into the experiment (Fig. 6). The individual “units” of this nanostructure
400 are ca. 50-100 nm in diameter. The distal side of the distal shield does not show this
401 nanostructure. Differences between the proximal and distal sides of the distal shield
402 have previously been reported (Henriksen et al 2004, Young et al 2004). Whereas the
403 distal side of the distal shield consists of crystallographic a-faces, the proximal side
404 seems to be more profoundly regulated by the cell and does not show crystallographic
405 faces (Young et al 2004). The nanostructure shown here is what was described as
406 “tuberculate surface” by Henriksen et al. (2004). The latter authors conclude that the
407 tubercles are part of the calcite structure. We confirm this conclusion which is illustrated
408 particularly well by a side view of these tubercles (Fig. 3D). We can only speculate what
409 effect this nanostructure might have on the dissolution resistance / susceptibility of the
410 distal shield elements. Considering that the distal shield elements of *C. braarudii* are the
411 only coccolith parts of all three species that are still present at the end of the experiment
412 (Fig. 6), it seems clear that they are comparatively dissolution resistant. Whether this
413 resistance stems from the nanostructure or some other feature remains an open question
414 but it is fair to say that the nanostructure does not make coccolith crystals highly
415 susceptible to dissolution. The importance of micro- and nanostructures in differential
416 dissolution behaviour of various biominerals has been recently highlighted in the

417 context of vulnerability to ocean acidification (Langer and Ziveri 2025). It is
418 conceivable that the nanostructure in *C. braarudii* slows down etching and / or provides
419 structural reinforcement. This scenario would be plausible if the nanostructure was an
420 organo-mineral composite structure as opposed to being composed of calcite only
421 (Walker and Langer 2021). A nanostructure of similar size in CaCO₃ biominerals is
422 widespread in extracellular calcifiers, where it is a central indicator of a layered growth
423 mechanism featuring particle accretion which is believed to be non-operative in
424 coccolithophores (Kadan et al 2021, Walker and Langer 2021). It remains, however, an
425 open question whether the nanostructure in *C. braarudii* is similar to that in
426 extracellular calcifiers i.e. whether it is also an organo-mineral composite structure
427 (Walker and Langer 2021). This question is pertinent to coccolithophore
428 biomineralization because an extracellular-like nanostructure in coccoliths would call
429 into question widely held views about crystallization of coccolith crystals (Walker and
430 Langer 2021). However, even if the tuberculate nanostructure in *C. braarudii* should
431 turn out to be extracellular-like, it would still be unclear how it is possible that the distal
432 side of the distal shield is different, i.e. shows crystallographic a-faces and no
433 nanostructure. The standard biomineralization model explaining the nanostructure in
434 extracellular calcifiers cannot account for the difference between the two sides of the
435 distal shield in *C. braarudii*, and neither can the standard model of coccolith
436 biomineralization (Young et al 2004, Walker and Langer 2021). This difference between
437 the proximal and the distal side of the distal shield shows how finely tuned
438 morphogenesis in *C. braarudii* is. We can only speculate how this fine tuning is
439 achieved, but the composition of the organic coating might play a role. The composition
440 of coccolith associated polysaccharides is known to be species specific, but we
441 speculate that it might also be site specific within the coccolith vesicle (Walker et al
442 2018b).

443 **4) Conclusions**

444 In summary, our results show that dissolution experiments complement field studies and
445 contribute to a deeper understanding of both coccolith structure and the ecological
446 impact of seawater undersaturation with respect to calcite. We conclude that

447 1) the most dissolution-resistant species is *C. braarudii*, followed by *H. carteri* and *S.*
448 *apsteinii*;

449 2) structural integrity of the coccosphere under dissolution is highest in *C. braarudii*,
450 followed by *H. carteri* and *S. apsteinii*, with *C. leptoporus* probably showing the
451 weakest coccosphere;

452 3) we identify dissolution in published field data where it was not recognised;

453 4) lopadolith R-units dissolve faster than V-units, illustrating that different
454 microstructures in the same coccolith have different dissolution kinetics despite
455 containing the same mineral;

456 5) the nanostructure in the distal shield of *C. braarudii* points to a fine-tuning in
457 coccolith morphogenesis that is not accounted for by our current model of coccolith
458 biomineralization.

459

460 **Acknowledgements**

461 We thank Martin Gachenot for technical assistance.

462 **Funding:**

463 Generalitat de Catalunya (MERS, 2021 SGR00640), Spanish Ministry of Science and
464 Innovation (CEX2019-000940-M), and BIOCAL project (PID2020-113526RB-I00,
465 Spanish Ministry of Science and Innovation). DFG project BONITOS 541693727.

466 **Competing interests**

467 The authors declare no conflict of interests.

468 **Author contributions**

469 GL: conception, experiments, analysis, writing, IP: experiments, writing, JRY: analysis,
470 field samples, writing, PZ: writing.

471 **Data availability**

472 All data are available in the Supplement.

473

474 **References**

475 Baumann, K.-H., Böckel, B., and Frenz, M.: Coccolith contribution to South Atlantic
476 carbonate sedimentation, in: Coccolithophores, edited by: Thierstein, H. R. and Young,
477 J. R., Springer Berlin Heidelberg, Berlin, Heidelberg, 367–402,
478 https://doi.org/10.1007/978-3-662-06278-4_14, 2004.

479 Berger WH (1973) Deep-sea carbonates: evidence for a coccolith lysocline. *Deep-Sea*
480 *Res* 20:917–921

481 Bianco, S., Bordiga, M., Langer, G., Ziveri, P., Cerino, F., Di Giulio, A., and Lupi, C.
482 (2025) Low sensitivity of a heavily calcified coccolithophore under increasing CO₂: the
483 case study of *Helicosphaera carteri*, *Biogeosciences*, 22, 1821–1837,
484 <https://doi.org/10.5194/bg-22-1821-2025>.

485 Broecker, W. & Clark, E. Ratio of coccolith CaCO₃ to foraminifera CaCO₃ in late
486 Holocene deep sea sediments. *Paleoceanogr.* 24, PA3205 (2009).

487 Broecker, W. S. & Peng, T.-H. *Tracers in the Sea*. 690 (Lamont-Doherty Geological
488 Observatory, Columbia University, 1982)

489 Broerse, A.T.C., Ziveri, P., Honjo, S., (2000) Coccolithophore (CaCO₃) flux in the Sea
490 of Okhotsk: seasonality, settling and alteration processes *Marine Micropaleontology*, 39
491 (1-4): 179-200.

492 Burns, D. A. (1977). Phenotypes and dissolution morphotypes of the genus
493 *Gephyrocapsa* Kamptner and *Emiliana huxleyi* (Lohmann). *New Zealand Journal of*
494 *Geology and Geophysics*, 20(1), 143-155.

495 Cubillos, J.C., Henderiks, J., Beaufort, L., Howard, W.R., & Hallegraeff, G.M. (2012).
496 Reconstructing calcification in ancient coccolithophores: Individual coccolith weight
497 and morphology of *Coccolithus pelagicus* (sensu lato). *Marine Micropaleontology*, 92,
498 29-39.

499 Daniels, C., Poulton, A., Young, J., Esposito, M., Humphreys, M., Ribas-Ribas, M.,
500 Tynan, E., and Tyrrell, T.: Species-specific calcite production reveals *Coccolithus*
501 *pelagicus* as the key calcifier in the Arctic Ocean, *Mar. Ecol. Prog. Ser.*, 555, 29–47,
502 <https://doi.org/10.3354/meps11820>, 2016.

503 Daniels, C. J., Sheward, R. M., and Poulton, A. J.: Biogeochemical implications of
504 comparative growth rates of *Emiliana huxleyi* and *Coccolithus* species,
505 *Biogeosciences*, 11, 6915–6925, <https://doi.org/10.5194/bg-11-6915-2014>, 2014.

506 Drescher B, Dillaman RM, Taylor AR. (2012) Coccolithogenesis In *Scyphosphaera*
507 *apsteinii* (Prymnesiophyceae). *J Phycol.* 2012 Dec;48(6):1343-61. doi: 10.1111/j.1529-
508 8817.2012.01227.x. Epub 2012 Sep 17. PMID: 27009987.

509 Gafar, N. A., Eyre, B. D., and Schulz, K. G.: Particulate inorganic to organic carbon
510 production as a predictor for coccolithophorid sensitivity to ongoing ocean acidification,
511 *Limnol. Oceanogr. Letters*, 4, 62–70, <https://doi.org/10.1002/lol2.10105>, 2019

512 Gerecht AC, Supraha L, Edvardsen B, Langer G, Henderiks J. 2015. Phosphorus
513 availability modifies carbon production in *Coccolithus pelagicus* (Haptophyta). *Journal*
514 *of Experimental Marine Biology and Ecology* 472: 24–31.

515 Gupta, .M., Banerjee, R. & Mergulhao, L. On the nature of the calcareous substrate of
516 a ferromanganese crust from the Vityaz Fracture Zone, Central Indian Ridge: (2002).
517 inferences on paleoceanography. *Geo-Mar Lett* 22, 12–18 (2002).
518 <https://doi.org/10.1007/s00367-002-0091-0>

519 Hassenkam, T., Johnsson, A. M. S., Bechgaard, K., & Stipp, S. L. S. (2011). Tracking
520 single coccolith dissolution with picogram resolution and implications for CO₂
521 sequestration and ocean acidification. *Proceedings of the National Academy of Sciences*
522 *of the United States of America*, 108, 8571-8576.

523 Henderiks, J., Sturm, D., Šupraha, L., & Langer, G. (2022). Evolutionary Rates in the
524 Haptophyta: Exploring Molecular and Phenotypic Diversity. *Journal of Marine Science*
525 *and Engineering*, 10(6), 798. <https://doi.org/10.3390/jmse10060798>

526 Henriksen, K., Young, J. R., Bown, P. R., & Stipp, S. L. S. (2004). Coccolith
527 biomineralisation studied with atomic force microscopy. *Palaeontology*, 47(3), 725-743.

528 Hoffmann, R., Kirchlechner, C., Langer, G., Wochnik, A. S., Griesshaber, E., Schmahl,
529 W. W., and Scheu, C. (2015) Insight into *Emiliana huxleyi* coccospheres by focused ion
530 beam sectioning, *Biogeosciences*, 12, 825–834, <https://doi.org/10.5194/bg-12-825-2015>,
531 2015.

532 Holcová K, Scheiner F. (2023). An experimental study on post-mortem dissolution and
533 overgrowth processes affecting coccolith assemblages: A rapid and complex process.
534 *Geobiology*. 2023 Mar;21(2):193-209. doi: 10.1111/gbi.12528. Epub 2022 Oct 11.
535 PMID: 36218003.

536 Honjo,S. 1975. "DISSOLUTION OF SUSPENDED COCCOLITHS IN THE DEEP-
537 SEA WATER COLUMN AND SEDIMENTATION OF COCCOLITH OOZE",
538 *Dissolution of Deep-sea Carbonates*, William V. Sliter, Allan W. H. Bé, Wolfgang H.
539 Berger

540 Johns, CT et al. Adsorptive exchange of coccolith biominerals facilitates viral infection.
541 *Sci. Adv.*9, eadc8728(2023). DOI:10.1126/sciadv.adc8728

542 Johnson, R., Langer, G., Rossi, S., Probert, I., Mammone, M., & Ziveri, P. (2022).
543 Nutritional response of a coccolithophore to changing pH and temperature. *Limnology*
544 *and Oceanography*, 67(10), 2309-2324.

545 Kadan Y, Tollervey F, Varsano N, Mahamid J, Gal A. (2021) Intracellular nanoscale
546 architecture as a master regulator of calcium carbonate crystallization in marine
547 microalgae. *Proc Natl Acad Sci U S A*. 2021 Nov 16;118(46):e2025670118. doi:
548 10.1073/pnas.2025670118. PMID: 34772804; PMCID: PMC8694050.

549 Keller, M. D., Selvin, R. C., Claus, W., & Guillard, R. R. (1987). Media for the culture
550 of oceanic ultraphytoplankton 1, 2. *Journal of phycology*, 23(4), 633-638.

551 Kleijne, A. (1990). Distribution and malformation of extant calcareous nannoplankton
552 in the Indonesian Seas. *Marine Micropaleontology*, 16(3-4), 293-316.

553 Langer, G. & Benner, I. (2009) Effect of elevated nitrate concentration on calcification
554 in *Emiliania huxleyi*. *J. Nannoplankton Res.* 30: 77–80.

555 Langer, G., & Bode, M. (2011). CO₂ mediation of adverse effects of seawater
556 acidification in *Calcidiscus leptoporus*. *Geochemistry, Geophysics, Geosystems*, 12(5).
557 <https://doi.org/10.1029/2010GC003393>

558 Langer, G., Geisen, M., Baumann, K. H., Kläs, J., Riebesell, U., Thoms, S., & Young, J.
559 R. (2006). Species-specific responses of calcifying algae to changing seawater
560 carbonate chemistry. *Geochemistry, geophysics, geosystems*, 7(9).

561 Langer, G., Gussone, N., Nehrke, G., Riebesell, U., Eisenhauer, A., Kuhnert, H., Rost,
562 B., Trimborn, S., & Thoms, S. (2006b). Coccolith strontium to calcium ratios in
563 *Emiliana huxleyi*: The dependence on seawater strontium and calcium concentrations.
564 *Limnology and Oceanography*, 51(1 I), 310-320.
565 <https://doi.org/10.4319/lo.2006.51.1.0310>

566 Langer, G., Nehrke, G., & Jansen, S. (2007). Dissolution of *Calcidiscus leptoporus*
567 coccoliths in copepod guts? A morphological study. *Marine Ecology Progress Series*,
568 331, 139-146.

569 Langer, G., Oetjen, K., Brenneis, T. (2013). On culture artefacts in coccolith
570 morphology. *Helgoland Marine Research*, 67(2), 359-369.
571 <https://doi.org/10.1007/s10152-012-0328-x>

572 Langer G, Taylor AR, Walker CE, Meyer EM, Ben Joseph O, Gal A, Harper GM,
573 Probert I, Brownlee C, Wheeler GL. Role of silicon in the development of complex
574 crystal shapes in coccolithophores. *New Phytol.* 2021 Sep;231(5):1845-1857. doi:
575 10.1111/nph.17230. Epub 2021 Mar 9. PMID: 33483994.

576 Langer G, Probert I, Cox MB, Taylor A, Harper GM, Brownlee C, Wheeler G. (2023)
577 The Effect of cytoskeleton inhibitors on coccolith morphology in *Coccolithus braarudii*
578 and *Scyphosphaera apsteinii*. *J Phycol.* 2023 Feb;59(1):87-96. doi: 10.1111/jpy.13303.
579 Epub 2022 Dec 24. PMID: 36380706.

580 Langer G. & Ziveri P. (2025) Vulnerability to ocean acidification of marine calcifying
581 organisms cannot be predicted from the mineral type in their shells. *Limnology and*
582 *Oceanography Letters* 10(4): 448-452. <https://doi.org/10.1002/lo12.70020>

583 Matsuoka, H. (1990) A new method to evaluate dissolution of CaCO₃ in the deep-sea
584 sediments. *Trans. Proc. Paleont. Soc. Jpn.*, 157, 430-434

585 McIntyre A, McIntyre R (1971) Coccolith concentration and differential solution in
586 oceanic sediments. In: Funnel BM, Riedel WR (eds) *The micropaleontology of oceans*.
587 Cambridge University Press, Cambridge, p 253–261

588 Meyer, Erin M., Langer, Gerald, Brownlee, Colin, Wheeler, Glen L. and Taylor, Alison
589 R. 2020 Sr in coccoliths of *Scyphosphaera apsteinii*: Partitioning behavior and role in
590 coccolith morphogenesis. *Geochimica et Cosmochimica Acta*, 285. 41-54.
591 10.1016/j.gca.2020.06.023

592 Milliman, J. D. Production and accumulation of calcium carbonate in the ocean: budget
593 of a nonsteady state. *Glob. Biogeochemical Cycles* 7, 927–957 (1993).

594 Morse, J. W. & Mackenzie, F. T. *Geochemistry of sedimentary carbonates*. (Elsevier,
595 1990).

596 Pierrot, D., D. Wallace, E. Lewis, R. Wallace, and W. Wallace. (2011) MS Excel
597 Program Developed for CO₂ System Calculations. ORNL Environmental Sciences
598 Division. doi:10.3334/CDIAC/otg

599 Roth PH, Berger WH (1975) Distribution and dissolution of coccoliths in the south and
600 central Pacific. In: Sliter WV, Be AWH, Berger WH (eds) CaCO₃ dissolution in the
601 deep sea. Cushman Foundation for Foraminiferal Research, Santa Barbara, CA, p 87–
602 113

603 Roth, P. H., & Coulbourn, W. T. (1982). Floral and solution patterns of coccoliths in
604 surface sediments of the North Pacific. *Marine Micropaleontology*, 7(1), 1–52.
605 doi:10.1016/0377-8398(82)90014-7

606 Sand, K., Pedersen, C., Sjoberg, S., Nielsen, J., Makovicky, E., and Stipp, S. (2014).
607 Biomineralization: long-term effectiveness of polysaccharides on the growth and
608 dissolution of calcite. *Cryst. Growth Des.* 14, 5486–5494. doi: 10.1021/cg5006743

609 Subhas, A. V., Rollins, N. E., Berelson, W. M., Erez, J., Ziveri, P., Langer, G., & Adkins,
610 J. F. (2018). The dissolution behavior of biogenic calcites in seawater and a possible
611 role for magnesium and organic carbon. *Marine Chemistry*, 205, 100–112.
612 <https://doi.org/10.1016/j.marchem.2018.08.001>

613 Subhas, A. V., Dong, S., Naviaux, J. D., Rollins, N. E., Ziveri, P., Gray, W., Rae, J. W.
614 B., Liu, X., Byrne, R. H., Chen, S., Moore, C., Martell-Bonet, L., Steiner, Z., Antler, G.,
615 Hu, H., Lunstrum, A., Hou, Y., Kemnitz, N., Stutsman, J., ... Adkins, J. F. (2022).
616 Shallow Calcium Carbonate Cycling in the North Pacific Ocean. *Global*
617 *Biogeochemical Cycles*, 36(5). <https://doi.org/10.1029/2022GB007388>

618 Sulpis, O., Jeansson, E., Dinauer, A., Lauvset, S. K., & Middelburg, J. J. (2021).
619 Calcium carbonate dissolution patterns in the ocean. *Nature Geoscience*, 14(6), 423–
620 428. <https://doi.org/10.1038/s41561-021-00743-y>

621 Walker JM, Langer G. (2021) Coccolith crystals: Pure calcite or organic-mineral
622 composite structures? *Acta Biomater.* 2021 Apr 15;125:83-89. doi:
623 10.1016/j.actbio.2021.02.025. Epub 2021 Feb 22. PMID: 33631395.

624 Walker JM, Greene HJM, Moazzam Y, Quinn PD, Parker JE, Langer G. (2024) An
625 uneven distribution of strontium in the coccolithophore *Scyphosphaera apsteinii*
626 revealed by nanoscale X-ray fluorescence tomography. *Environ Sci Process Impacts.*
627 2024 Jun 19;26(6):966-974. doi: 10.1039/d3em00509g. PMID: 38354057.

628 Walker CE, Taylor AR, Langer G, Durak GM, Heath S, Probert I, Tyrrell T, Brownlee
629 C, Wheeler GL. (2018a) The requirement for calcification differs between ecologically
630 important coccolithophore species. *New Phytol.* 2018 Oct;220(1):147-162. doi:
631 10.1111/nph.15272. Epub 2018 Jun 19. PMID: 29916209; PMCID: PMC6175242.

632 Walker, Charlotte E., Heath, Sarah, Salmon, Deborah L., Smirnoff, Nicholas, Langer,
633 Gerald, Taylor, Alison R., Brownlee, Colin and Wheeler, Glen L. (2018b) An
634 extracellular polysaccharide-rich organic layer contributes to organization of the
635 coccosphere in coccolithophores. *Frontiers in Marine Science*, 5 (AUG), [306].
636 (doi:10.3389/fmars.2018.00306).

637 Wheeler GL, Sturm D, Langer G. (2023) *Gephyrocapsa huxleyi* (*Emiliana huxleyi*) as a
638 model system for coccolithophore biology. *J Phycol.* 2023 Dec;59(6):1123-1129. doi:
639 10.1111/jpy.13404. Epub 2023 Nov 20. PMID: 37983837.

640 Yang M, Batchelor-McAuley C, Barton S, Rickaby REM, Bouman HA, Compton RG.
641 (2021) Opto-Electrochemical Dissolution Reveals Coccolith Calcium Carbonate
642 Content. *Angew Chem Int Ed Engl.* 2021 Sep 13;60(38):20999-21006. doi:
643 10.1002/anie.202108435. Epub 2021 Aug 15. PMID: 34288323; PMCID:
644 PMC8518593.

645 Young, J. R. (1994). Variation in *Emiliana huxleyi* coccolith morphology in samples
646 from the Norwegian EHUX experiment, 1992. *Sarsia.* 79(4): 417-425.

647 Young, J. R. (2008). *Scyphosphaera porosa* Kamptner 1967 rediscovered in the
648 plankton. *Journal of Nannoplankton Research.* 30(1): 35-38

649 Young, J. R., Henriksen, K., & Probert, I. (2004). Structure and morphogenesis of the
650 coccoliths of the CODENET species. In *Coccolithophores: From molecular processes to*
651 *global impact*, Thierstein, H. R., & Young, J. R. (Eds.), Springer, 191-216.

652 Ziveri, P., Baumann, K.H., Böckel, B. Bollmann, J. and Young, J. (2004) Present day
653 coccolithophore-biogeography in the Atlantic Ocean in Thierstein, H. and Young, J.
654 Eds. Coccolithophores: From Molecular Processes to Global Impact. Springer Verlag:
655 403-428.

656 Ziveri, P., De Bernardi, B., Baumann, K.-H., Stoll, H. M., and Mortyn, P. G.: Sinking of
657 coccolith carbonate and potential contribution to organic carbon ballasting in the deep
658 ocean, Deep-Sea Res. Pt. II, 54, 659–675, <https://doi.org/10.1016/j.dsr2.2007.01.006>,
659 2007.

660 Ziveri, P., Gray, W. R., Anglada-Ortiz, G., Manno, C., Grelaud, M., Incarbona, A., Rae,
661 J. W. B., Subhas, A. V., Pallacks, S., White, A., Adkins, J. F., & Berelson, W. (2023).
662 Pelagic calcium carbonate production and shallow dissolution in the North Pacific
663 Ocean. Nature Communications, 14(1), 805. <https://doi.org/10.1038/s41467-023-36177->
664 w

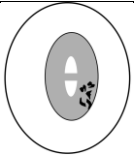
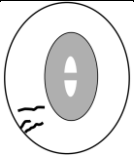
665 Ziveri, P., Passaro, M., Incarbona, A., Milazzo, M., Rodolfo-Metalpa, R., & Hall-
666 Spencer, J. M. (2014). Decline in Coccolithophore Diversity and Impact on Coccolith
667 Morphogenesis Along a Natural CO₂ Gradient. The Biological Bulletin, 226(3), 282–
668 290. <https://doi.org/10.1086/BBLv226n3p282>

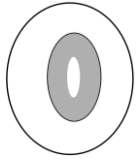
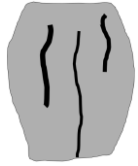
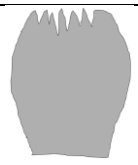
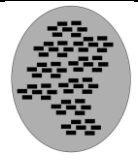
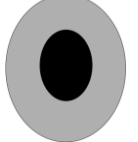
669

670 TABLES

671 Table 1. Summary of important dissolution features.

672

| coccolith | dissolution feature | sketch |
|---------------------|--------------------------|---|
| <i>C. braarudii</i> | etching of inner tube |  |
| <i>C. braarudii</i> | etching of distal shield |  |

| | | |
|------------------------------------|-----------------------------|---|
| <i>C. braarudii</i> | central area bar missing |  |
| <i>H. carteri</i> | etching |  |
| <i>S. apsteinii</i> lopadoliths | etching of barrel |  |
| <i>S. apsteinii</i> lopadoliths | serrated rim |  |
| <i>S. apsteinii</i> muroliths | etching |  |
| <i>S. apsteinii</i> muroliths | centre missing |  |

673

674

675 FIGURE CAPTIONS

676 Fig 1 *Coccolithus braarudii*

677 A) coccosphere at t0, no dissolution. Scale bar 5µm. B) coccosphere; etching (e) of tube
678 and distal shield and central area bar missing (b). Scale bar 5µm. C) broken coccoliths
679 (bc), etching of tube, central bar missing and gaps in coccosphere. Scale bar 5µm. D)
680 collapsed coccosphere (c), also showing etching (e) of tube and distal shield and central
681 area bar missing (b). Scale bar 5µm. E) coccolith, etching (e) of tube and distal shield,
682 and central area bar missing (b). Note that the etching consistently occurs by opening of
683 sutures between elements rather than by dissolution of element surfaces. Scale bar 3µm.

684

685 Fig 2 *Coccolithus braarudii*

686 A) broken coccolith (bc) distal shield in distal view. B) broken coccolith proximal view
687 of distal shield showing nanostructure (ns); the arrow indicates isolated distal shield
688 elements in distal view, from another coccolith, not displaying nanostructure (nns) on
689 distal and vertical surfaces. All scale bars 2 μ m.

690

691 Fig 3 *Coccolithus braarudii*

692 A) broken coccolith distal shield in proximal view showing nanostructure (ns). Scale
693 bar 2 μ m B) proximal view of distal shield elements showing nanostructure (ns). Scale
694 bar 500nm. C) proximal view of distal shield elements showing nanostructure (ns);
695 individual "tubercles" (t) of the nanostructure are ca 50-100nm, Scale bar 200nm. D)
696 isolated distal shield elements showing nanostructure "tubercles" (t) in vertical side
697 view (arrow). Scale bar 200nm.

698

699 Fig 4 *Helicosphaera carteri*

700 A) coccosphere at t₀, no dissolution. Scale bar 5 μ m. B) coccosphere displaying
701 coccoliths with severe etching (e) and a broken coccolith (bc). Scale bar 5 μ m. C)
702 collapsed coccosphere including broken coccoliths (bc). Scale bar 5 μ m. D) coccoliths in
703 distal view with etching (e) in flange and blanket. Scale bar 3 μ m. E) coccolith in distal
704 view with etching in flange and blanket. Scale bar 2 μ m. F) coccolith in proximal view
705 with etching (e) in flange. Scale bar 5 μ m.

706

707 Fig 5 *Scyphosphaera apsteinii*

708 A) coccosphere at t₀, no dissolution B) lopadolith base etching (be); muralith centre
709 missing (cm) C) lopadolith barrel etching (re) and serrated rim (sr) D and E) broken
710 lopadoliths F) isolated V-units G) muralith at t₀, no dissolution H) muralith with
711 etching (me) I) lopadolith in distal view showing R- and V-units (R- and V arrows,
712 Young 2008); and broken muralith (bm). All scale bars 5 μ m.

713

714 Fig 6 Timelines of dissolution. Bars indicate the period during which the respective
715 feature can be observed. Shaded backgrounds indicate the onset points of major
716 features. Pink backgrounds indicate the onset of etching, blue backgrounds indicate the
717 onset of breakage/collapse. For example-images of each feature see Figs 1-5.

718

719 Fig 7 Quantification of the observations illustrated in Fig 6. Plotted is the percentage of
720 each analysed feature versus time in hours from start of experiment. A) *Scyphosphaera*
721 *apsteinii* lopadoliths B) *Scyphosphaera apsteinii* muraliths C) *Helicosphaera carteri* D)
722 *Coccolithus braarudii*

723

724 Fig 8 Field samples showing etching patterns comparable to those seen in the
725 experimental samples (arrows). All scale bars 2 μm .

726 *Coccolithus braarudii*: A) Lower surface of a broken piece of distal shield showing
727 nanostructure. B) Central area of distal shield showing early stage dissolution. C)
728 Proximal surface showing advanced dissolution.

729 *Helicosphaera carteri*: D) Distal Surface showing early stage dissolution. E) Proximal
730 surface showing advanced dissolution.

731 A, B - sediment trap samples from 3200m, N. Atlantic; C - surface water sample, NW
732 Atlantic; D- sediment trap sample, Canaries, 200m; E plankton sample from 120m, Gulf
733 of Mexico.

734

735

Fig 1

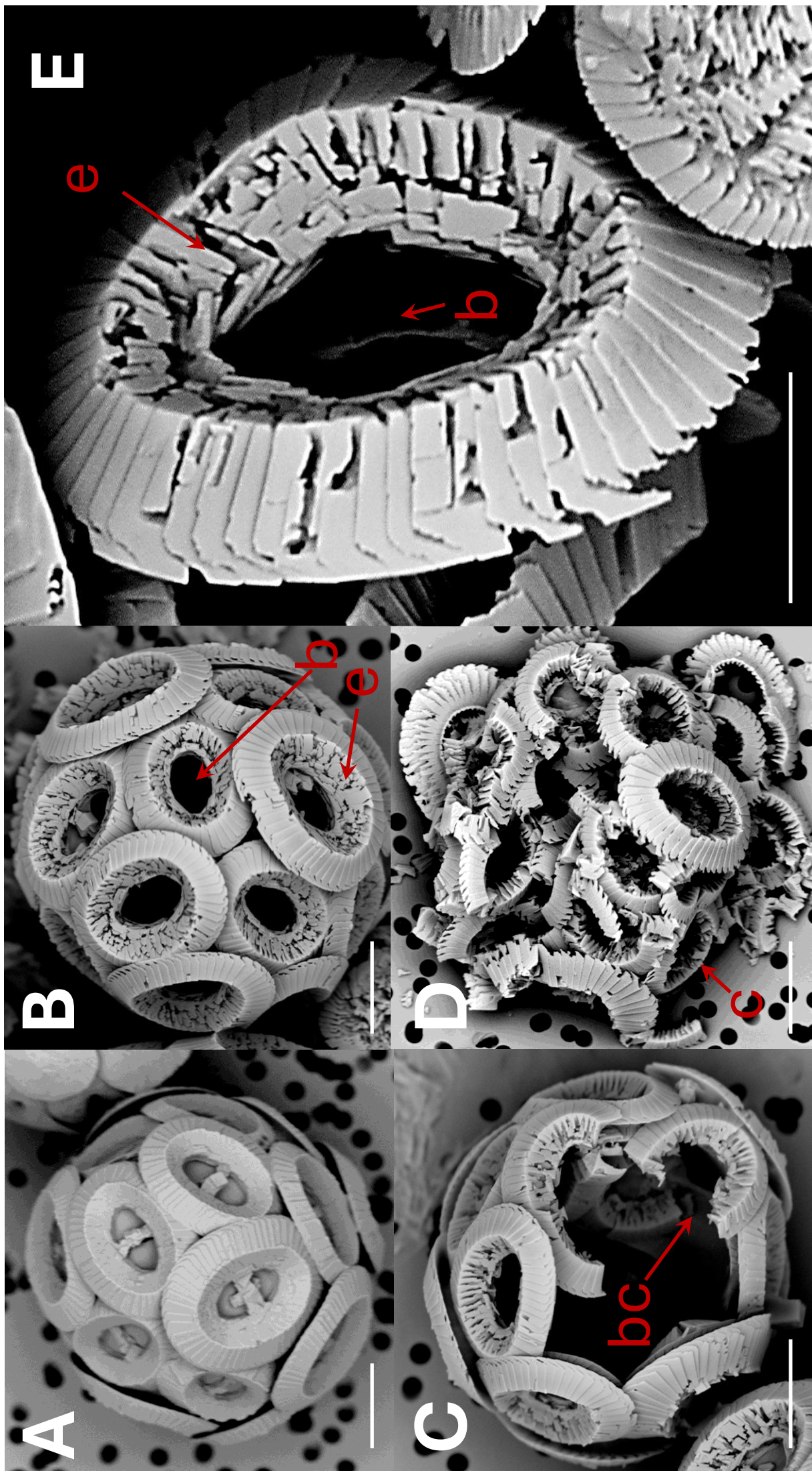


Fig 2

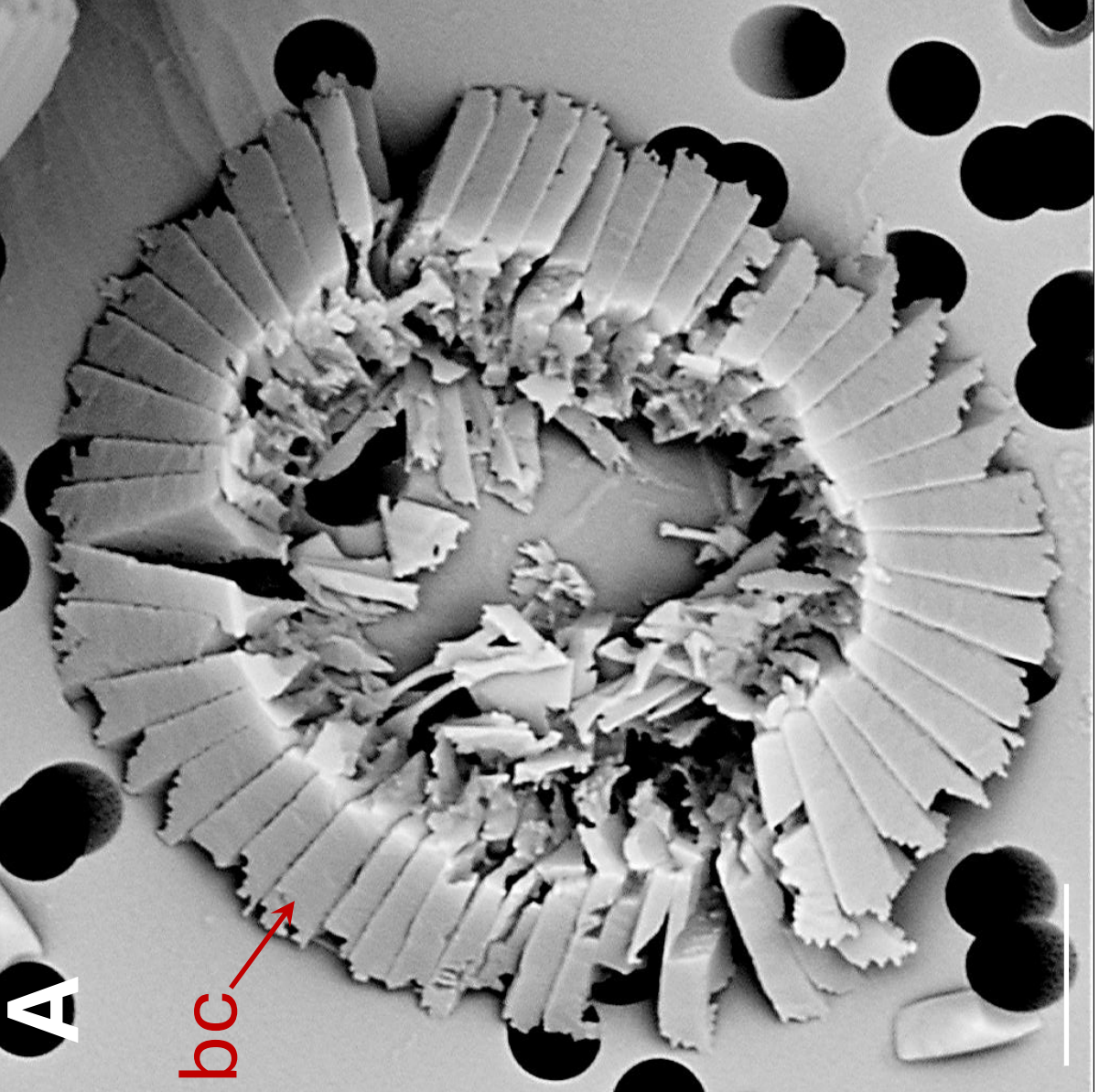
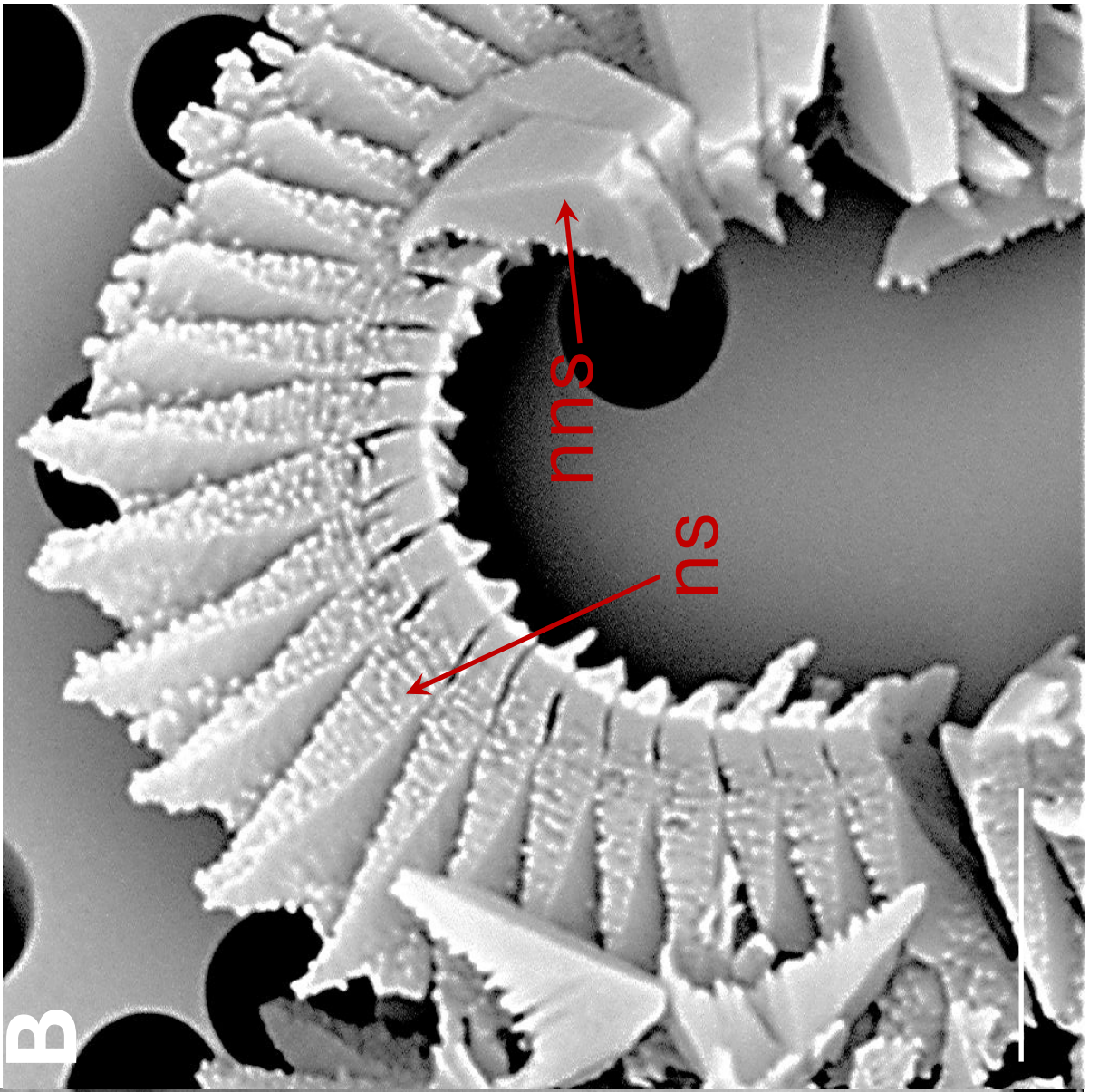


Fig 3

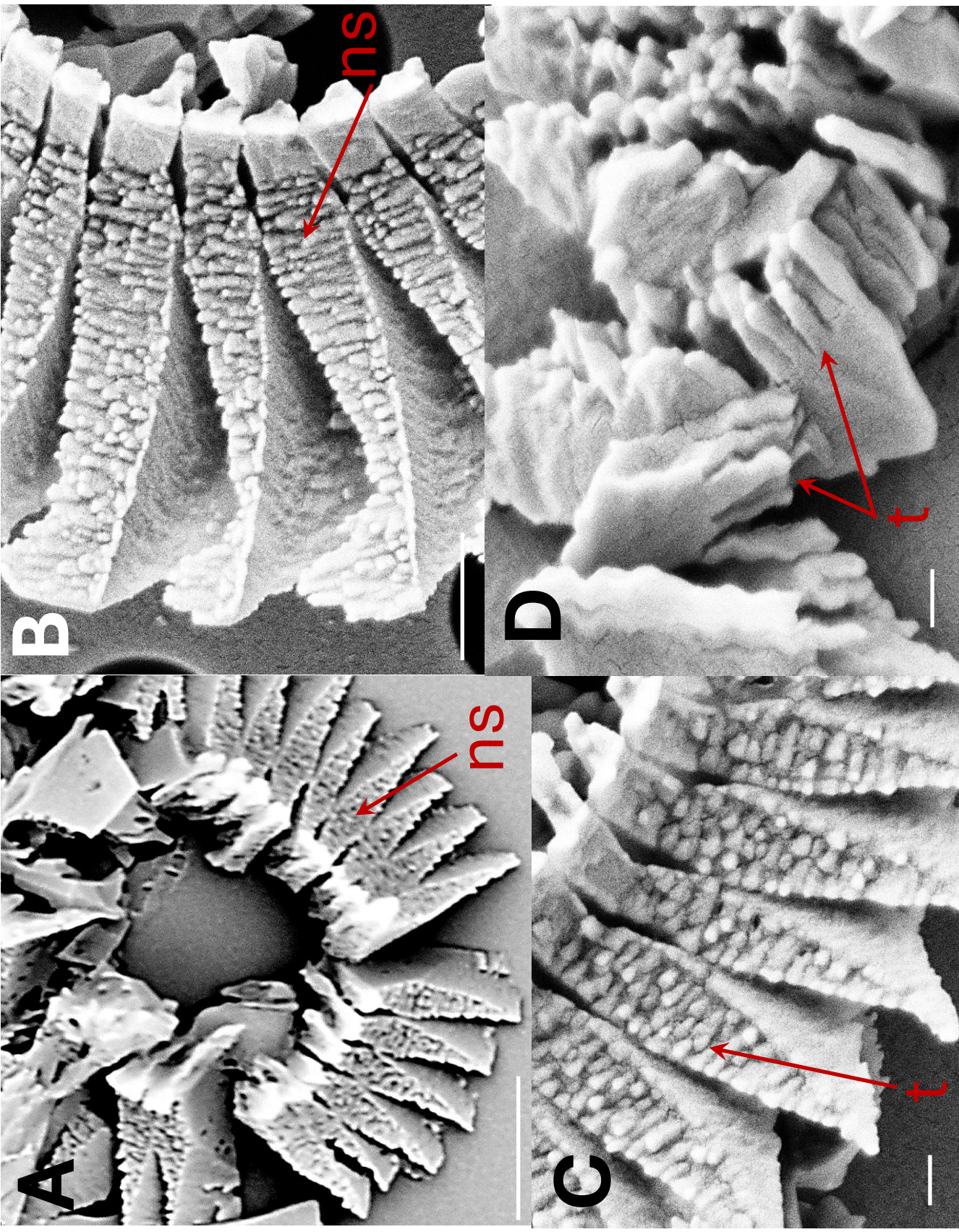


Fig 4

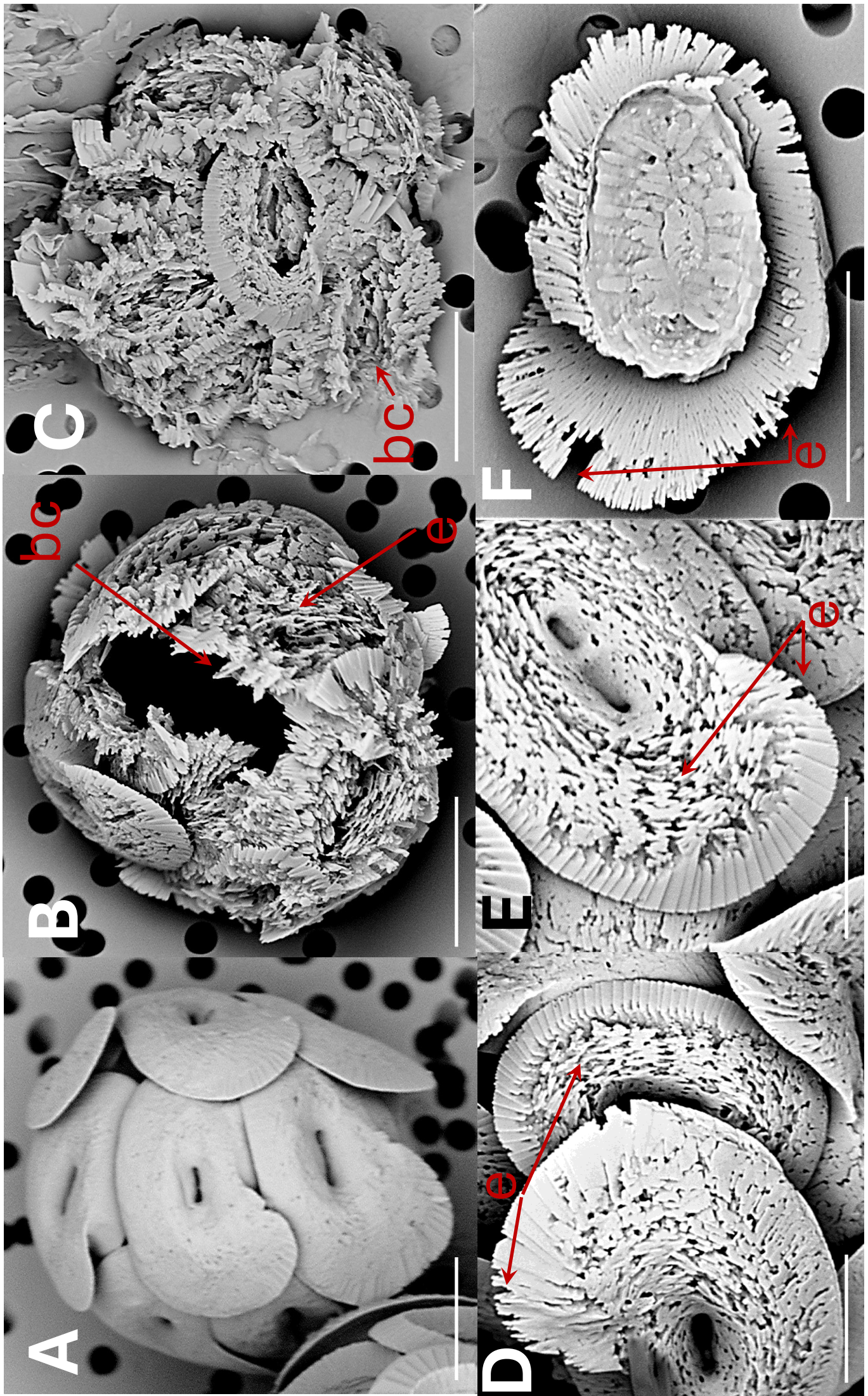


Fig 5

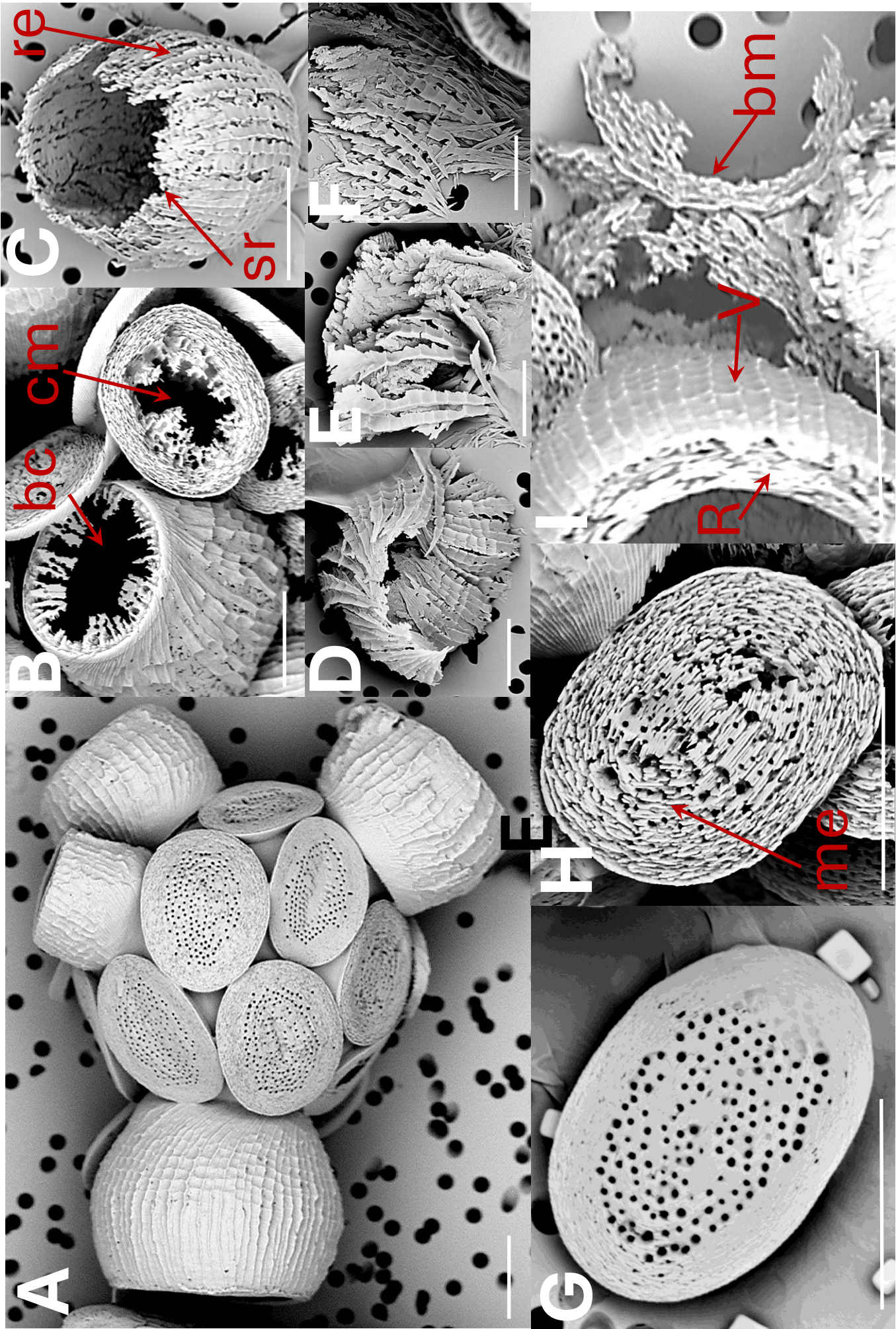
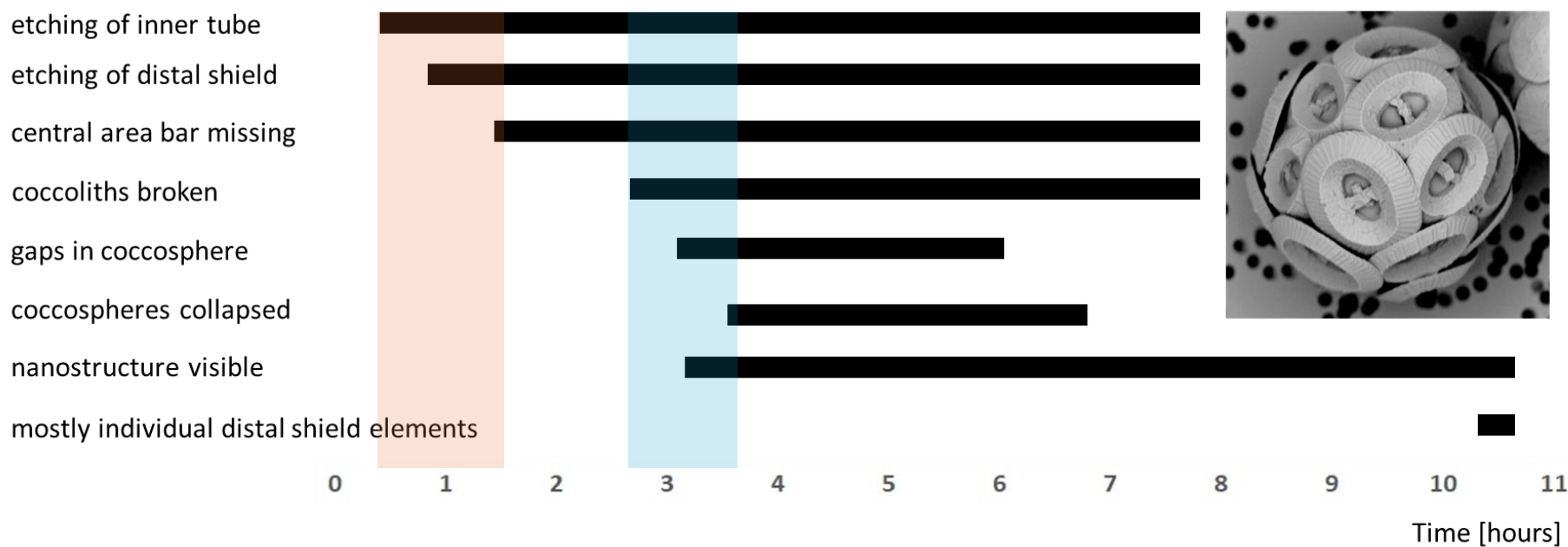


Fig 6

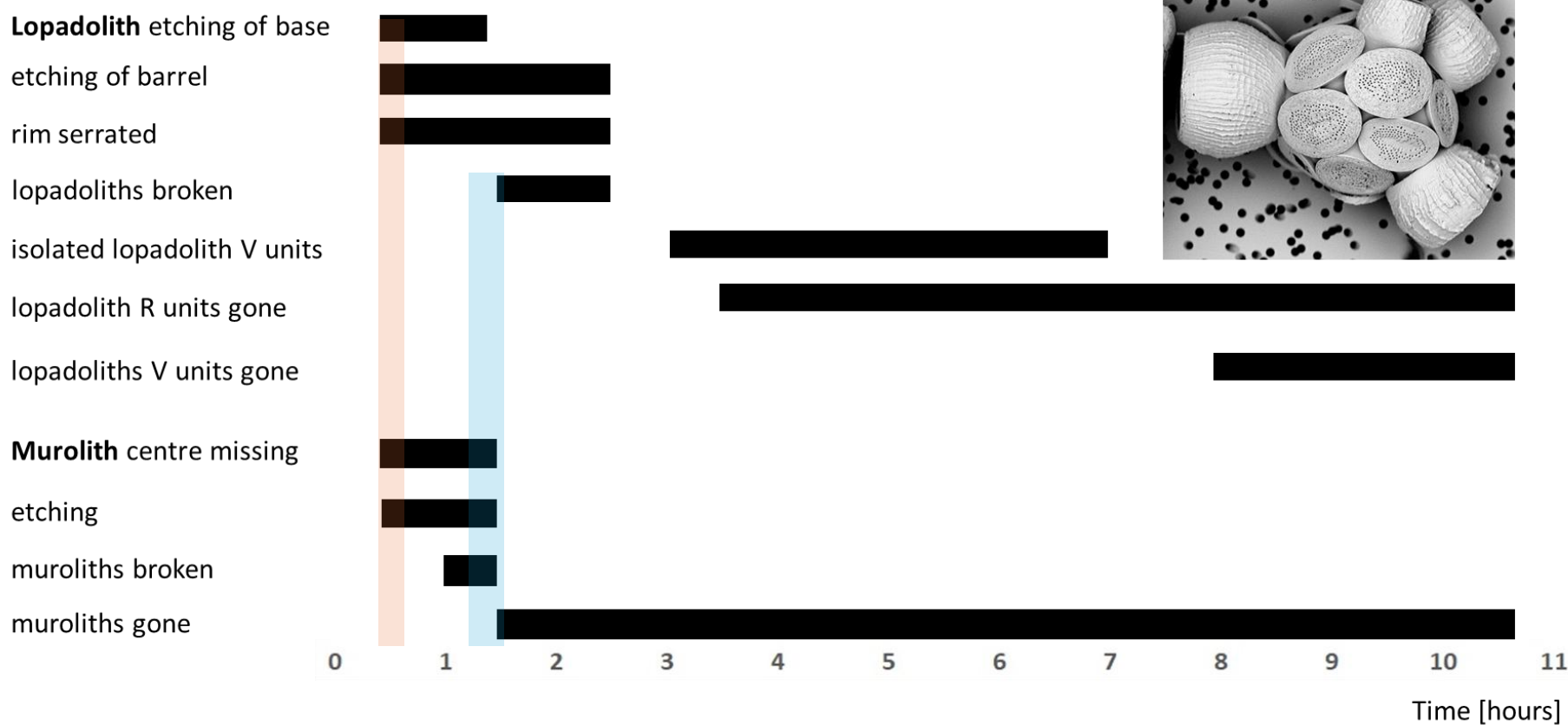
Coccolithus braarudii



Helicosphaera carteri



Scyphosphaera apsteinii



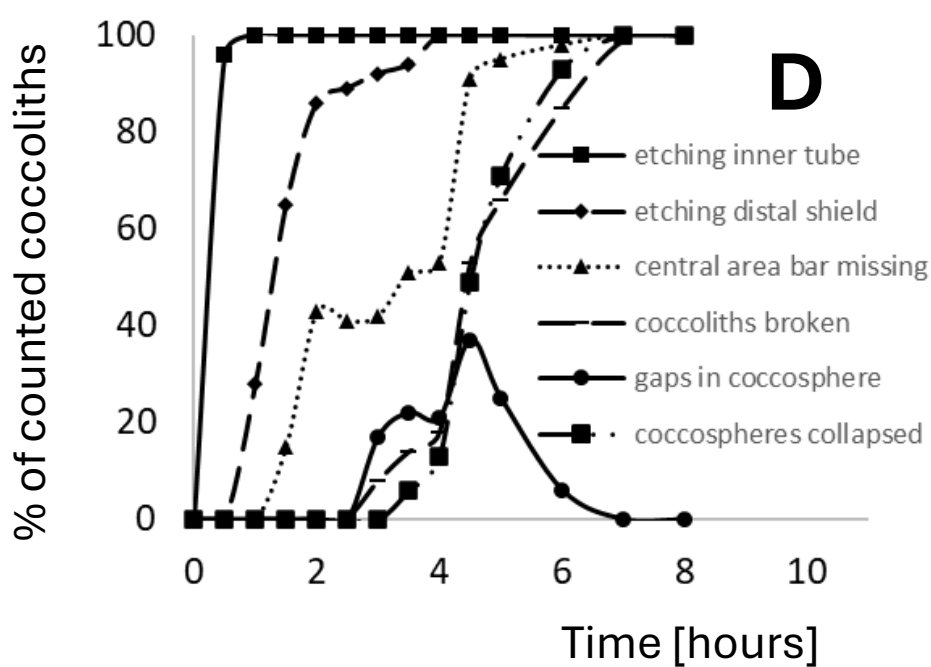
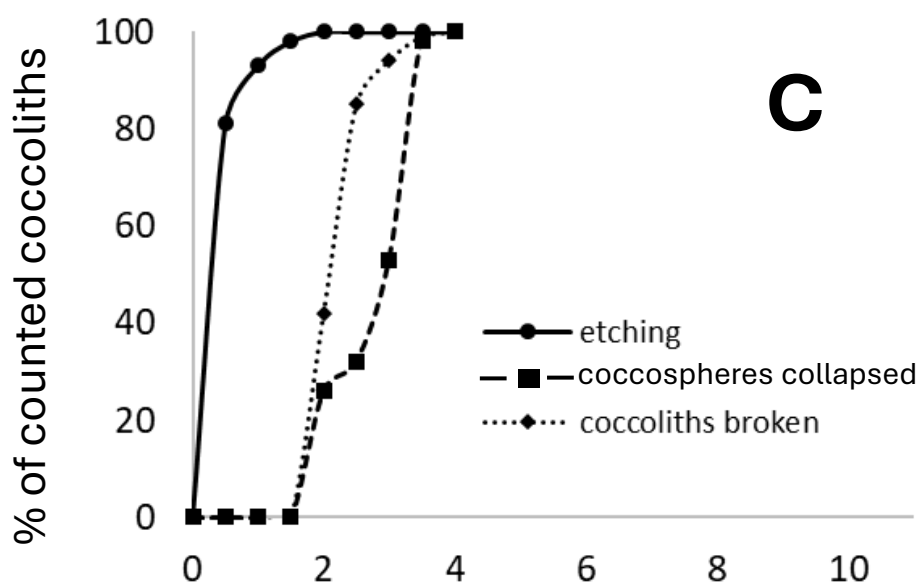
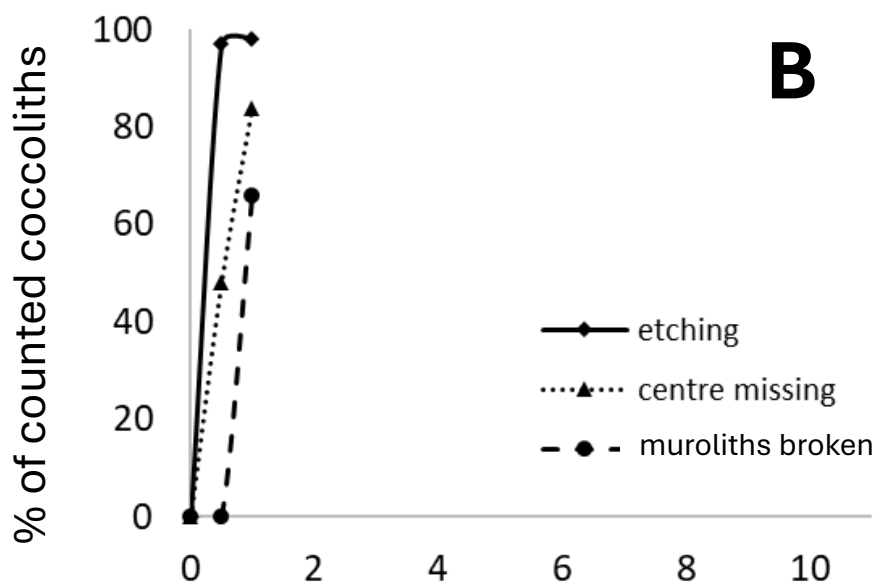
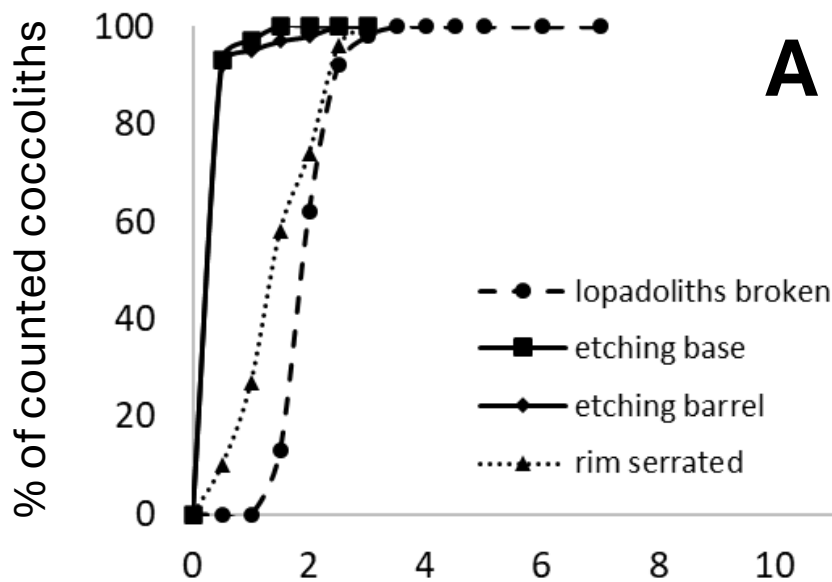


Fig 8

